Accessory factors promote AlfA-dependent plasmid segregation by regulating filament nucleation, disassembly, and bundling

Jessica K. Polka[a], Justin M. Kollman[b], and R. Dyche Mullins[a,1]

[a]Department of Cellular and Molecular Pharmacology, University of California, San Francisco, CA 94158; and [b]Department of Anatomy and Cell Biology, McGill University, Montreal, QC, Canada H3A 2B2

Edited by James A. Spudich, Stanford University School of Medicine, Stanford, CA, and approved December 30, 2013 (received for review March 4, 2013)

In bacteria, some plasmids are partitioned to daughter cells by assembly of actin-like proteins (ALPs). The best understood ALP, ParM, has a core set of biochemical properties that contributes to its function, including dynamic instability, spontaneous nucleation, and bidirectional elongation. AlfA, an ALP that pushes plasmids apart in *Bacillus*, relies on a different set of underlying properties to segregate DNA. AlfA elongates unidirectionally and is not dynamically unstable; its assembly and disassembly are regulated by a cofactor, AlfB. Free AlfB breaks up AlfA bundles and promotes filament turnover. However, when AlfB is bound to the centromeric DNA sequence, *parN*, it forms a segrosome complex that nucleates and stabilizes AlfA filaments. When reconstituted in vitro, this system creates polarized, motile comet tails that associate by antiparallel filament bundling to form bipolar, DNA-segregating spindles.

DNA segregation | bacterial cytoskeleton | *Bacillus subtilis* | reconstitution

The first filament-forming actin-like protein (ALP) was identified in bacteria in 2001 (1), and subsequent work identified more than 30 additional classes of ALPs in eubacteria and archaea (2). These proteins are involved in a variety of cellular processes, including assembly of the cell wall (1, 3–5), positioning of organelles (6), anchoring of cytokinesis machinery (7), and segregation of DNA (8). Most DNA-segregating ALPs participate in type II plasmid partitioning systems, which consist of three components: (*i*) a centromeric DNA sequence; (*ii*) a DNA-binding protein that interacts with the centromeric sequence to form a segrosome complex; and (*iii*) a polymer-forming ALP, whose self-assembly moves the segrosome through the cytoplasm (*SI Appendix*, Fig. S1). In the best understood type II segregation system, bidirectional polymerization of the ALP, ParM, pushes pairs of plasmids to opposite poles of rod-shaped cells. Extensive studies, both in vivo and in vitro, have produced detailed models of ParM-mediated DNA segregation (9, 10), but it is unclear to what extent these models can be generalized to describe other ALP-dependent DNA segregation systems.

To better understand the diversity of molecular mechanisms underlying plasmid segregation, we studied a type II plasmid partitioning system encoded by the *alf* operon from the *Bacillus subtilis* plasmid pLS32 (11). The *alf* operon was first identified based on its ability to maintain plasmids through the process of sporulation, presumably by actively pushing a plasmid into the forespore at one end of the cell. In addition, the *alf* operon confers approximately eightfold greater stability to plasmids in rapidly dividing cells. The *alf* operon itself contains a centromeric sequence, *parN*, with three short, repeated sequences, and it encodes both an ALP, AlfA, and a DNA-binding protein, AlfB. The AlfA protein shares 15% sequence identity with ParM (2), whereas AlfB shares only 8% identity with ParR and has no significant BLAST hits (expect value < 1). In addition to sequence differences, AlfA and ParM also differ biochemically. ParM filaments are dynamically unstable and do not form bundles in the absence of molecular crowding agents. AlfA, in contrast, displays no evidence of dynamic instability and forms stable filaments that self-assemble into mixed-polarity bundles, even in high salt concentrations (12, 13). The dynamic instability of ParM filaments is thought to play an important role in plasmid segregation, in part by providing the energy required to move the plasmids in a directed fashion. Energy must be expended to disassemble unneeded filaments and raise the concentration of monomers above the critical concentration required to elongate cargo-attached filaments. Otherwise, monomer and polymer reach a stable, steady-state ratio, and directed motion ceases. In eukaryotic cells, several proteins, including the actin-binding proteins cofilin and profilin, collaborate to maintain a high concentration of monomeric actin, orders of magnitude higher than the critical concentration for polymerization. In bacteria, the dynamic instability of unattached ParM filaments maintains the concentration of monomeric ParM approximately fourfold above the critical concentration of filaments attached to segrosomes (9, 14). If assembly of AlfA filaments drives plasmid movement, then how, in the absence of dynamic instability, is the concentration of monomeric AlfA maintained at a level sufficient to drive the growth of segrosome-attached filaments? To understand how AlfA filaments assemble and move DNA, we followed AlfA-dependent plasmid segregation in vivo and reconstituted the process in vitro using purified components. Like the par system, the *alf* system relies on assembly of actin-like polymers to push plasmids, but the two systems use different sets of underlying molecular mechanisms to favor the assembly of cargo-attached filaments over free filaments. AlfB binds to *parN* DNA, creating a segrosome complex that nucleates AlfA

Significance

Many bacteria contain large, circular DNA molecules, called plasmids, that encode physiologically, medically, and commercially important genes, including genes conferring virulence and drug resistance. The largest plasmids use active segregation systems to maintain themselves in the host bacterium. Such segregation systems provide remarkable insight into bacterial cell biology. The pLS32 plasmid, found in a commercially important strain of *Bacillus subtilis*, relies on a segregation system encoded by the *alf* operon. We show that DNA movement is driven by self-assembly of a polymeric protein, called AlfA, and that self-assembly of AlfA into a functional, DNA-segregating machine requires the activity of the accessory factor AlfB, which (unexpectedly) promotes both assembly and disassembly of AlfA polymers.

Author contributions: J.K.P. and R.D.M. designed research; J.K.P. and J.M.K. performed research; J.K.P., J.M.K., and R.D.M. analyzed data; and J.K.P. and R.D.M. wrote the paper.

The authors declare no conflict of interest.

This article is a PNAS Direct Submission.

[1]To whom correspondence should be addressed. E-mail: dyche@mullinslab.ucsf.edu.

This article contains supporting information online at www.pnas.org/lookup/suppl/doi:10.1073/pnas.1304127111/-/DCSupplemental.

filaments and remains attached to their growing ends. Remarkably, however, the AlfB protein by itself also debundles and destabilizes AlfA filaments and maintains a high concentration of monomeric AlfA sufficient to drive plasmid movement. Once formed, AlfA filaments elongate in a polarized manner, from only one end, and binding of the segrosome complex increases filament stability, even in the presence of high concentrations of free AlfB. Together, these properties produce treadmilling AlfA "comet tails" that move DNA similar to the way polarized actin comet tails move cargo in eukaryotic cytoplasm. In sporulating cells, these monopolar comet tails would be sufficient to push plasmids into the forespore so that they would survive sporulation. In actively growing cells, antiparallel association of these comet tails can also segregate plasmids to opposite poles and decrease the rate of plasmid loss.

Results

AlfA Forms Dynamic Filaments in Vivo That Push Plasmids. To study AlfA-driven cargo movement in *B. subtilis* cells, we constructed miniplasmids containing both the replication origin and *alf* operon from plasmid pLS32 (15). We inserted a second copy of the AlfA gene at the end of the native *alf* operon. The additional gene encodes an AlfA-GFP fusion protein and enables us to express both WT and fluorescently labeled AlfA in the same cells. In our construct, AlfA-GFP is present at 25% of the level of WT AlfA, whereas, in a similar, previously published strain (11), AlfA-GFP is present at 7% (*SI Appendix*, Fig. S2). Although expression of AlfA-GFP decreases the efficiency of the *alf* operon by approximately twofold, the modified *alf* operon remains functional and confers a fourfold increase in stability over plasmids lacking an *alf* operon altogether (*SI Appendix*, Table S4). We therefore used this construct to follow AlfA dynamics in vivo (Fig. 1). Consistent with previous reports (11), we found that AlfA forms filamentous structures that move, grow, and shorten on a timescale of approximately 1 min. The majority of cells do not contain a single, cell-spanning filament, but rather contain multiple, discrete bundles that frequently fragment, diffuse, and anneal with one another (Fig. 1*A*). These observations are surprising, given our previous demonstration that purified AlfA forms stable filament bundles (12), and they suggest that additional factors dynamize the filaments.

We visualized plasmids containing a lacO array bound to chromosome-encoded mCherry-LacI and observed that some of them "surf" on the tips of elongating AlfA structures (Fig. 1*B*, frames beginning with *), similar to the way plasmids move on the ends of ParM spindles (16). Other plasmids, however, move linearly along preexisting AlfA polymers in a manner we never observed with ParM-driven plasmids (Fig. 1*B*, frames beginning with <). To quantify the population-level effects of the *alf* system on plasmid mobility, we used MicroTracker (17) to follow the movement of >500 plasmids over time. Surprisingly, plasmids carrying the *alf* operon are less mobile than controls, but the character of their motion is less diffusive and more directed. In plots of mean squared displacement vs. time (Fig. 1*C*), the exponential scaling factor that describes plasmid motion (α) is significantly increased by the presence of the *alf* operon, suggesting that plasmid motions are influenced by an active process (18). We next worked to figure out how accessory factors regulate the stability of AlfA filament bundles (12) and promote directed motion of plasmids.

Regulation of AlfA Polymer Dynamics by Elements of the *alf* Operon: AlfB and *parN*. The *alf* operon contains three potential ORFs: AlfA, AlfB, and AlfC. Two have been shown to encode proteins important for plasmid segregation: AlfA and AlfB. Loss of the third, AlfC, has little effect on plasmid stability (19). The AlfB protein is thought to bind three DNA repeats in the *parN* locus and form a kinetochore-like segrosome structure (19) that

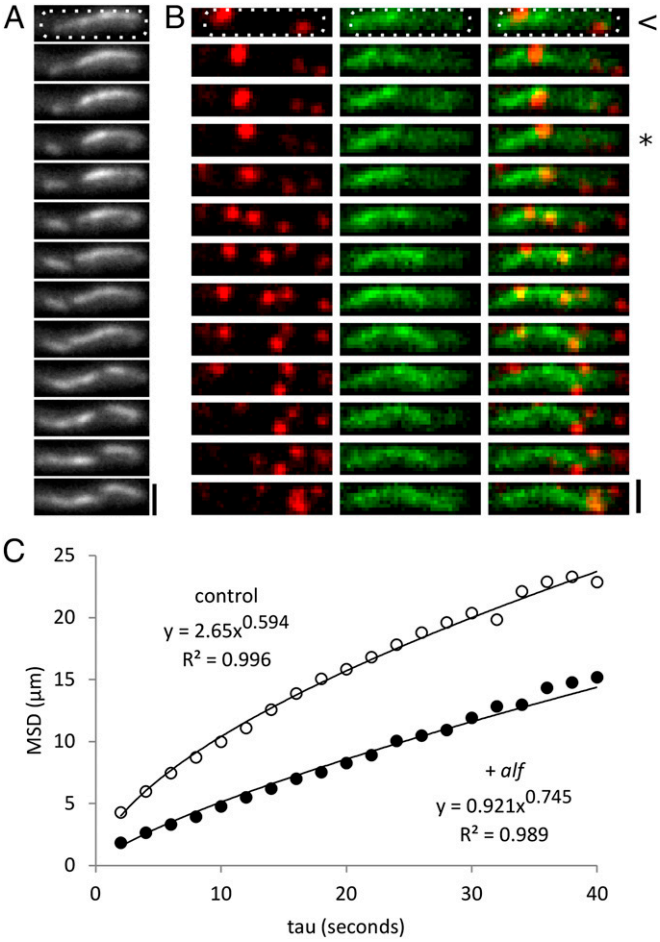

Fig. 1. AlfA forms dynamic filaments in vivo that push plasmids. (*A*) AlfA bundles from pNCH106 in PY79 form a dynamic polymer network in the cell. This sequence contains examples of growth, shortening, fragmentation, and apparent annealing. Time between images: 10 s. (Scale bar, 1 μm.) Temperature, 30 °C. Cell outline shown in white dashed line. (*B*) pJKP06 plasmids (red) track along the sides and ends of growing AlfA bundles (green) in PY79 cells, and these motions can separate pairs of plasmids. Interval, 5 s. (Scale bar, 1 μm.) Temperature, 25 °C. Cell outline shown in white dashed line. Frames indicating transit along preexisting filaments begin with <, and those indicating tip surfing begin with *. (*C*) Mean squared displacement (MSD) of trajectories of plasmids with (pJKP06, $n = 570$) and without (pJKP02, $n = 612$) the *alf* system shows that *alf* plasmids have decreased mobility (a reduced apparent diffusion coefficient) but a more directed character of motion (an increased exponential scaling factor, α). Temperature, 25 °C.

interacts with AlfA filaments. If free AlfB helps regulate AlfA polymer dynamics, independent of its role in the segrosome, we would expect its cellular concentration to be much higher than that of the AlfB binding sites in *parN*, which we estimate to be ~25 nM (15). We would, instead, expect the AlfB concentration to be comparable to that of AlfA. The concentration of AlfA, in turn, should be higher than the critical concentration for its polymerization (2.4 μM) (12). To find out whether this is case, we used quantitative immunoblotting to estimate the concentrations of AlfA and AlfB in *Bacillus* cells (*SI Appendix*, Fig. S3). Consistent with a role outside the segrosome, we found that the ratio of AlfB to AlfA is quite high (~1:2). We estimate the AlfA concentration to be 20 μM in the *B. subtilis* cell, whereas AlfB is present at ~8 μM. In contrast, the estimated concentrations of ParM and ParR are, respectively, ~15 and <1 μM (8).

We next used right-angle light scattering to follow kinetics of AlfA assembly in the presence of various concentrations of AlfB

(Fig. 2*A*). Substoichiometric concentrations of AlfB (<12% of AlfA concentration) have little effect on the kinetics of polymer assembly, suggesting that AlfB by itself does not promote nucleation or severing of AlfA filaments. Low concentrations of AlfB do, however, dramatically reduce the intensity of the light scattering signal at steady state. Light scattering by AlfA is dominated by large filament bundles (12) so AlfB might decrease steady-state scattering because it antagonizes AlfA bundling, even at these low stoichiometries. We confirmed this by electron microscopy (Fig. 2*D*), which reveals both a dramatic decrease in the number of AlfA bundles (Fig. 2*C*) and an overall shortening of filament and bundle lengths in the presence of AlfB. How does AlfB reduce the bundling of AlfA filaments? Two simple possibilities are that AlfB either (*i*) binds to the sides of AlfA filaments and prevents their lateral association or (*ii*) decreases the lifetime of AlfA filaments so that they do not survive long enough to be incorporated into bundles. Consistent with both roles for AlfB, we find that it has no effect on AlfA bundles formed in the presence of the slowly hydrolyzable nucleotide analog ATPγS (*SI Appendix*, Fig. S5*B*). This insensitivity suggests that AlfB promotes disassembly of filaments that have hydrolyzed their bound ATP, or that AlfB cannot promote the disassembly of bundled filaments. Higher concentrations of AlfB (≥40% of the AlfA concentration) begin to reduce the rate of polymerization, suggesting that AlfB might—with low affinity—also cap AlfA filaments or sequester AlfA monomers. Consistent with low affinity sequestration, we found that AlfB increases the critical concentration of AlfA in a concentration-dependent manner (*SI Appendix*, Table S5) and that AlfB binds to monomeric AlfA (*SI Appendix*, Fig. S6).

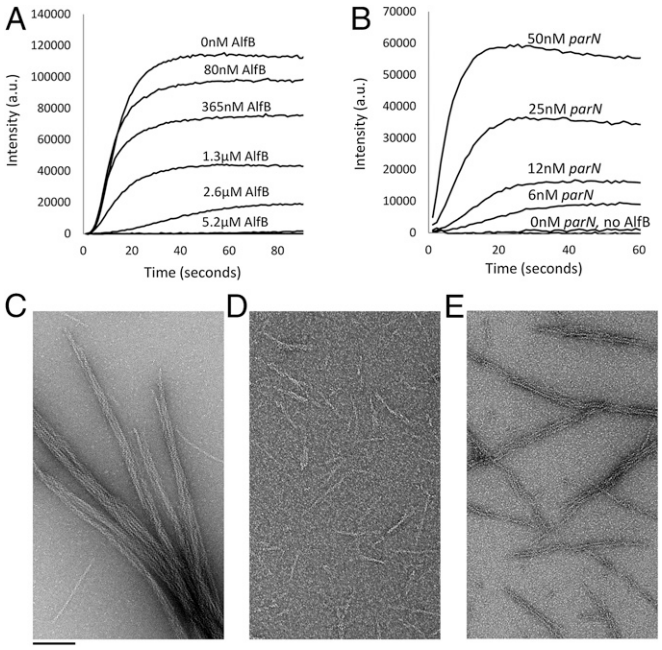

Fig. 2. AlfB and the *parN*/AlfB segrosome complex regulate stability and self-association of AlfA filaments. (*A*) Increasing concentrations of AlfB destabilize 3.3 μM AlfA polymerized in the presence of 2.5 mM ATP. Buffer, 25 mM Tris, pH 7.5, 100 mM KCl, 1 mM $MgCl_2$, and 1 mM DTT. (*B*) Increasing concentrations of *parN* promote polymerization of 2 μM AlfA in the presence of 1.3 μM AlfB. This concentration of AlfA does not support polymerization without *parN* even in the absence of AlfB (bottom trace; 5 mM ATP). Buffer as above. (*C*) AlfA alone forms regular bundles. Electron micrographs of negatively stained 4 μM AlfA polymerized with 2 mM ATP alone. Buffer as above. (*D*) AlfB debundles AlfA polymer and shortens the polymer length distribution (as above with 2 μM AlfB). Buffer as above. (*E*) The addition of both 2 μM AlfB and 60 nM *parN* restores bundles (as above with 60 nM *parN*). Buffer as above.

By contrast, addition of AlfB together with double-stranded DNA containing the centromeric *parN* sequence promotes AlfA polymerization at low concentrations, below those required for assembly of AlfA alone or in the presence of AlfB (Fig. 2*B*). That is, the *parN*/AlfB segrosome complex lowers the AlfA concentration required for filament assembly (*SI Appendix*, Table S5). In addition, *parN* promotes AlfA bundling in the presence of AlfB (Fig. 2*E*). Given that the number of AlfB binding sites introduced by *parN* (assuming binding of a dimer of AlfB to each of three repeats per molecule of *parN*) is a small fraction of the total concentration of AlfB (360 nM of 2 μM total), the increased bundling cannot be accounted for solely by a reduction in free AlfB. Because AlfB does not disrupt stable, preformed bundles (*SI Appendix*, Fig. S5*B*), *parN*-stabilized filaments likely form bundles because they survive long enough to interact with each other. These effects are observed only with *parN*-containing DNA, and not with nonspecific DNA (*SI Appendix*, Fig. S4).

Normalizing for the reduced critical concentration, we found that the segrosome complex abolishes the early lag phase of polymerization associated with spontaneous nucleation (Fig. 3*A*). On log-log plots (Fig. 3*A*, *Inset*), the segrosome decreases the slope of the initial phase of polymerization from ∼2 to ∼1, indicating that segrosome-mediated nucleation occurs in a single step (20) rather than the two steps required for spontaneous AlfA assembly (12). To test whether the number of AlfB binding sequences in *parN* is optimized for nucleation, we compared the rates of polymerization induced by WT *parN* with mutants containing various numbers of AlfB binding sites (*SI Appendix*, Table S6). Remarkably, *parN* constructs containing three tandem repeats induce the fastest rate of polymer assembly (Fig. 3*B*). Adding or removing binding sites significantly slows polymer assembly, even when the total concentration of all components (AlfA, AlfB, and AlfB binding sites) remains constant. Oddly, increasing the spacing between *parN* repeats further accelerates polymerization of AlfA and, judging from the steady-state light scattering signal, may increase polymer stability (*SI Appendix*, Fig. S5*A*). Decreasing the length of the linker or removing it entirely has only a small effect on assembly kinetics. These data suggest that, although the AlfB/*parN* segrosome complex nucleates rapid filament assembly, the *parN* locus has not evolved to promote the fastest assembly possible (21). Finally, we verified the sequence-specific binding of AlfB to *parN* (22) by electron microscopy of negatively stained samples (Fig. 3 *C* and *D*).

The nucleating and stabilizing activities of the segrosome complex suggest that it might bind to the ends of AlfA filaments. To localize the *parN*/AlfB complex on AlfA filaments, we coupled 10-nm colloidal gold-streptavidin conjugates to *parN*-biotin (*SI Appendix*, Table S6) and, to improve the clarity of our images, we generated an AlfA mutant with reduced bundling (*SI Appendix*, Fig. S7). We observed some particles associated with the sides of AlfA filaments (15/66, or 23% of filaments) but, in the majority of cases where we observed filaments associated with gold particles (48/66, or 73% of filaments), the particles are attached to only one end of the filament (Fig. 3*E*). We rarely observed segrosome complexes decorating both ends of an AlfA filament (3/66 or 5% of filaments), and this may be due to residual bundling activity of the mutant (∼5% of observed structures on EM grids are bundles) rather than symmetrical association of the segrosome with the filaments. To test this idea, we constructed stable AlfA seeds that we could distinguish from normal AlfA filaments in electron micrographs by decorating short, stabilized AlfA filaments with streptavidin. Seeds were assembled from 50% bundling-deficient AlfA mutant and 50% biotinylated WT AlfA (12). When seeds are elongated by 100% bundling-deficient AlfA in the presence of adenosine 5′-(β,γ-imido)triphosphate lithium salt hydrate (AMP-PNP), the majority (11/14 or 79%) grow preferentially from one end

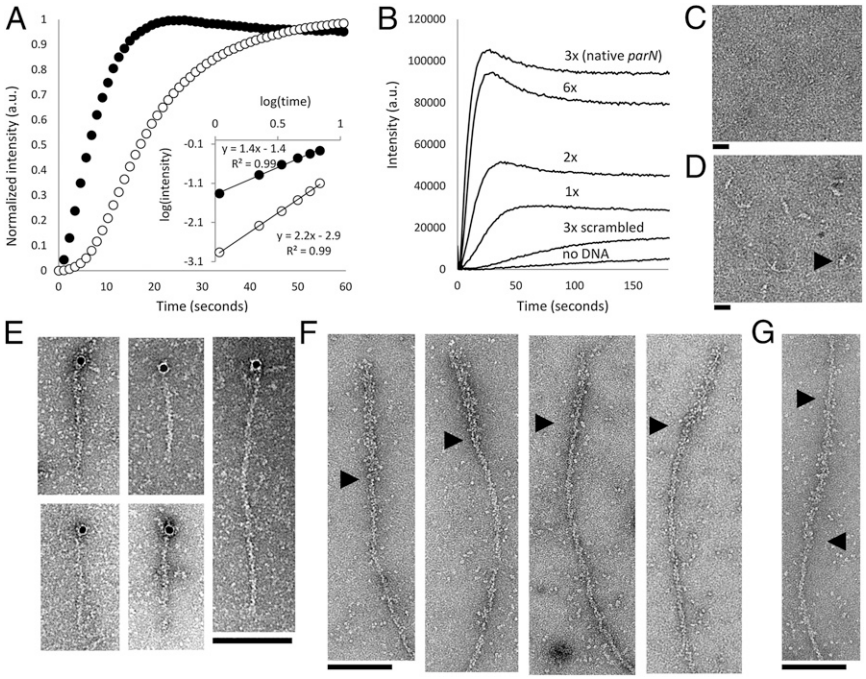

Fig. 3. AlfB forms a complex on *parN* DNA that nucleates AlfA polymerization and binds to the ends of polar filaments. (*A*) Intensity-normalized light scattering of 300 nM of AlfA polymer formed in the absence (○) and presence (●) of 1.3 μM AlfB and 50 nM *parN*. The nucleation-dominated lag phase of polymerization is dramatically reduced with AlfB and *parN*, and the change in the slope of early time points on a log-log plot indicates that the number of steps of polymer assembly is reduced (5 mM ATP). Buffer, 25 mM Tris, pH 7.5, 100 mM KCl, 1 mM $MgCl_2$, and 1 mM DTT. (*B*) Stabilization of AlfA by the *parN*/AlfB complex depends on the valency of AlfB-binding DNA repeats. Each reaction contains 2.1 μM AlfA, 1.3 μM AlfB, and 75 nM individual repeats. For example, the sequence containing a single repeat is present at 75 nM, whereas the native *parN* sequence, with three repeats, is present at 25 nM (2 mM ATP). Buffer as above. (*C*) 500 nM AlfB does not form a complex in the presence of 50 nM parC (the centromere of the ParM system). Buffer, 25 mM Tris, pH 7.5, 30 mM KCl, 10 mM $(NH_4)_2SO_4$, 1 mM DTT, and 1 mM EDTA. (Scale bar, 20 nM.) (*D*) A complex is formed in the presence of *parN*. (Scale bar, 20 nM.) Black arrowhead points to a representative complex. Buffer as above. (*E*) AlfB-*parN* binds to the ends of filaments; 10-nm colloidal gold particles coated in streptavidin localize predominantly to the ends of 3.5 μM AlfA KK21AA KK101AA filaments in the presence of 1.3 μM AlfB and 120 nM *parN*-biotin (2 mM ATP). Buffer, 25 mM Tris, pH 7.5, 100 mM KCl, 1 mM $MgCl_2$, and 1 mM DTT. (*F*) Filaments are polar. KK21AA KK101AA filaments (3 μM total monomer concentration) was polymerized off of AMP-PNP stabilized seeds composed of 50% KK21AA KK101AA AlfA and 50% AlfA-biotin decorated with an excess of streptavidin and diluted to 100 nM. Black arrowheads show boundaries between streptavidin-decorated seeds and normal filaments. Buffer as above. (*G*) A subset (21%) of these labeled filaments displays the seed in the middle. This configuration may be due to bundling of the WT polymer or streptavidin cross-linking within the seed. Buffer as above. Black arrowheads denote ends of the streptavidin seed.

(Fig. 3*F*). A small fraction of seeds grow from both ends (3/14 or 21%), possibly as a result of streptavidin cross-linking, residual bundling activity, or annealing (Fig. 3*G*).

Reconstitution of AlfA-Mediated DNA Movement and Segregation: Treadmilling of AlfA Bundles Produces Motile Comet Tails That Push DNA. We used total internal reflection fluorescence (TIRF) microscopy to watch assembly of AlfA filaments in the presence of AlfB-*parN* segrosome complexes. Using multivalent, streptavidin *parN*-Cy3 conjugates, we found that a 1:2 ratio of AlfB to AlfA supported formation of dynamic, polarized, comet tail structures that drive directed motion of DNA (Fig. 4 *A* and *B*). The segrosome complexes associate with the thick ends of tapered filament bundles, whose width and density decrease from the *parN*-associated end to the distal tip. At lower DNA concentrations, comet tails are longer and adhere more tightly to the glass surface. The increased adhesion revealed that DNA surfs processively on the elongating tips of comet tails (Fig. 4*C* and Movie S1). The morphology and dynamics of these structures indicate that the DNA-associated end is continuously assembling, whereas the free end is continuously disassembling. Thus, the filament destabilizing effect of free AlfB and the stabilizing effect of AlfB/*parN* segrosomes work together to promote preferential elongation of DNA-attached AlfA filaments and bundles and to generate sustained treadmilling of AlfA bundles. In addition to surfing growing ends, some *parN* particles also move processively along their lengths, probably propelled by association with the end of a filament growing along the bundle. Individual bundles can also support bidirectional movement (Fig. 4*C* and Movie S2). At higher DNA concentrations, individual DNA foci occasionally split, with the two components moving away in opposite directions along the bundle (Fig. 4*D* and Movie S3). At higher *parN* concentrations, comet tails are shorter, probably because the higher number of segrosome-associated AlfA comets compete for AlfA monomers. We frequently observed motile AlfA/segrosome structures undergoing complex rearrangements, including capture of adjacent structures by bundling, fragmentation of DNA particles on bifurcating bundles, and bidirectional DNA segregation (Fig. 4*E* and Movies S4 and S5). We observed a distinct bias toward bidirectional segregation, in that pairs of DNA particles attached to the same structure move apart at three times the frequency that they move together (*SI Appendix*, Table S7). This bias, together with previously reported reference-free averages of AlfA filament pairs (12), suggests that AlfA filaments have an inherent preference for antiparallel bundling.

Discussion

In our initial characterization of its assembly dynamics, we found that AlfA forms stable bundles, with no indication of dynamic instability (12). Given this, we wondered how segrosome-attached filaments could move cargo at steady state. That is, how is the assembly of segrosome-attached filaments privileged over that of

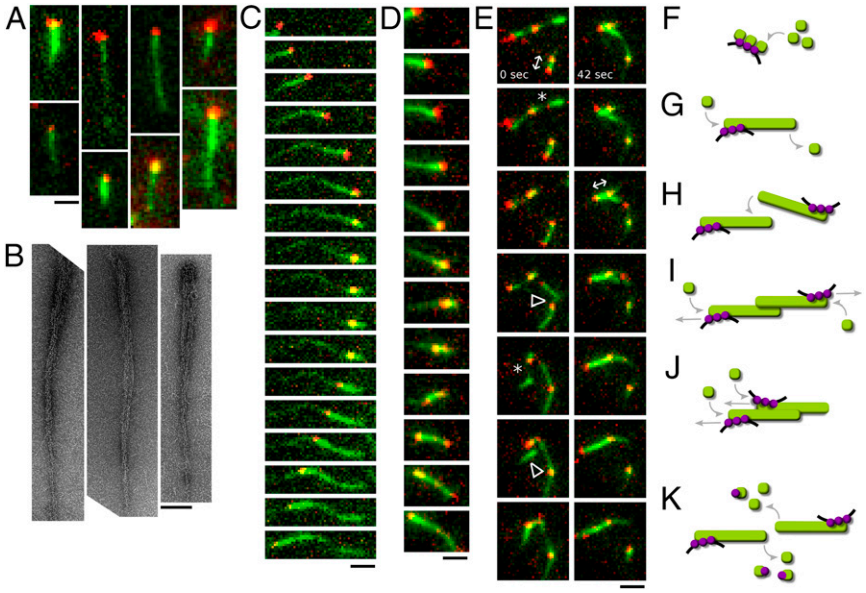

Fig. 4. Reconstitution of AlfA-mediated DNA segregation. Bundling of AlfA comet tails organizes DNA movements along a single axis. (*A* and *B*) In the presence of AlfB, AlfA polymers form comet tails behind multivalent *parN*-streptavidin conjugates. (*A*) These asymmetric structures can be visualized by TIRF microscopy. (Scale bar, 1 μm.) Buffer, 25 mM Tris, pH 7.5, 100 mM KCl, 1 mM $MgCl_2$, 1 mM DTT, 0.4% 400 CP methylcellulose, and 15 mg/mL BSA. (*B*) Asymmetric structures can also be seen with electron microscopy. (Scale bar, 100 nm.) Note the tapered appearance of the AlfA bundles. (3.2 μM AlfA, 1.6 μM AlfB, 60 nM *parN*). Buffer as above, without methylcellulose and BSA. (*C*) The growing end of an AlfA polymer pushes a *parN* conjugate. When the filament elongation ceases, the *parN* particle reverses direction and tracks backward along the original bundle ahead of new polymer growth, demonstrating that these bundles can support bidirectional movement (20 nM *parN*). (Scale bar, 1 μm.) Interval, 20 s. Buffer as in *A*. (*D*) A *parN* particle on the end of an AlfA polymer splits in two. One focus continues to track the growing filament tip, whereas the other reverses direction and moves backward along the bundle (60 nM *parN*). (Scale bar, 1 μm.) Interval, 12 s. Buffer as in *A*. (*E*) A group of AlfA bundles with multiple *parN* foci undergo complex rearrangements including bundle thinning and fragmenting (*), capture by annealing (Δ), and segregation by polymerization (↔) (60 nM *parN*). (Scale bar, 1 μm.) Interval, 6 s. Buffer as in *A*. (*F–K*) Model for AlfA-mediated segregation. (*F*) AlfA (green) polymer assembly occurs preferentially at *parN* (black)-AlfB (purple) complexes, which nucleate filaments below the critical concentration by coordinating AlfA monomers. (*G*) The *parN*-AlfB complex also stabilizes filaments beneath the AlfA critical concentration. (*H*) When filaments encounter one another, they may capture one another by bundling together. (*I*) Insertional polymerization of antiparallel bundles will push plasmids apart from one another. (*J*) Parallel bundles will not bring plasmids together, unless only the leading filament stalls. If the lagging filament stalls, plasmids will still be segregated. Therefore, assuming parallel and antiparallel bundling are equally likely, plasmids will tend to be segregated. (*K*) The range of paired plasmid movement is limited by filament turnover at ends free of AlfB-*parN*, with the debundling and sequestration activities of free AlfB promoting the turnover of AlfA filaments.

unattached filaments. Here we demonstrate that this problem is solved by the Alf B protein, which not only couples AlfA filaments to DNA but also destabilizes unattached AlfA filaments and bundles. The net effect is to raise the steady state concentration of AlfA monomers and promote preferential elongation of DNA-associated filament ends.

In addition to stabilizing attached AlfA filaments, the AlfB-*parN* segrosome complex also nucleates new filament formation. The efficiency of nucleation depends strongly on the number of AlfB-binding repeats in the DNA sequence, with the WT number of three repeats being optimal. This number of repeats might be related to the fact that the critical AlfA nucleus is composed of three monomers (12), but because the AlfB protein is likely a dimer, further biophysical studies will be required to understand the mechanism of segrosome-mediated nucleation. Interestingly, we find that increasing the spacing between AlfB-binding repeats in *parN* increases the efficiency of nucleation. Either (*i*) there is no selective advantage to faster nucleation or (*ii*) other functions of AlfB, such as transcriptional repression (19), dictate its spacing along the DNA.

Although AlfB promotes dissociation of AlfA bundles, segrosome-bound AlfA filaments form bundles even in the presence of excess AlfB. Because substoichiometric concentrations of *parN* can produce this effect, it is unlikely to be caused by depletion of free AlfB. Furthermore, because we only rarely observe gold-labeled *parN* conjugates decorating the sides of AlfA filaments, it is unlikely that the segrosome complex bundles filaments by cross-linking them along their lengths. Instead, we propose that bundling may be related to filament stability. We previously observed formation of bundles in vitro by slow, lateral association of AlfA filaments (12), and therefore we suggest that long-lived filaments have more time to find each other and form bundles. AlfB appears to destabilize AlfA filaments after they have hydrolyzed their bound ATP. This destabilization would undermine the stability of existing bundles and decrease the frequency with which filaments interact to form bundles in the first place. The AlfB/*parN* segrosome increases the stability of bound filaments and probably preserves them long enough to permit bundle formation. Based on our data, it is unclear whether bundling itself also increases the stability of AlfA polymers, but this is likely. Broadly, the role of bundling and molecular crowding in plasmid segregation systems needs to be investigated in greater detail, especially in light of recent studies of the ParM system (10).

The AlfB-*parN* segrosome binds preferentially to one end of AlfA filaments. This polarized association of the segrosome coupled with the destabilization of unbound ends dynamizes the system and promotes uni-directional treadmilling. Insertional polymerization can propel the DNA forward on the end of a growing comet tail or along the length of a preexisting structure through annealing of filaments. Based on these observations, we propose a simple model for AlfA-mediated plasmid movement and segregation (Fig. 4 *F–K*). Filament assembly is directed to plasmids by the nucleation and stabilization activity of AlfB-*parN*. This localized stabilization is sufficient to produce

linear structures capable of finding the long axis of rod-shaped *B. subtilis* cells (2, 16) and is likely sufficient to place the *alf*-containing plasmid, pLS32, in the forespore compartment of sporulating cells. This basic behavior probably underlies the dramatic increase in the rate at which *alf* operon-containing plasmids survive sporulation. When two plasmid-bound filaments encounter one another, they can bundle together. If the bundling is antiparallel, which appears to be the preferred interaction, further polymerization will drive the plasmids apart. If the bundling is parallel, the distance between plasmids will be maintained as both centromeres move in the same direction until the leading filament stalls. Furthermore, the disparity in filament stability at centromere-bound and unbound ends predicts that the range of these coordinated movements will be limited by filament turnover.

Thus, the *alf* system provides bacterial implementations of regulatory features familiar to eukaryotic actin, such as regulated nucleation, filament destabilization driven by a cofilin-like cofactor, filament treadmilling, and motile comet tail formation. Furthermore, the suppression and rescue of inherent bundling properties of AlfA may play a role in specifying physical associations between plasmid-bound polymers. These features expand our understanding of diversity in the regulation of bacterial polymers that move cellular cargoes.

Materials and Methods

Briefly, intracellular concentrations were calculated using values from the literature (23, 24). Plasmids for *B. subtilis* were constructed from a fragment from pWH1520 containing an *Escherichia coli* origin and ampicillin resistance gene, as well as a *B. subtilis* tetracycline resistance gene. This fragment was ligated to repN, the origin of replication from pLS32. To this backbone, the *alf* operon, a lacO array, and GFP from pMutin were added. Fluorescently tagged LacI constructs were cloned under a xlyose-inducible promoter into pSG1154 from the Pogliano laboratory, which integrates into AmyE. Constructs were transformed into PY79 for integration in the AmyE locus.

Live cell imaging of *B. subtilis* was performed as previously described (2). Images were acquired in oblique TIRF on a Nikon TE 2000 inverted microscope controlled with MicroManager (25) as previously described (12). Plasmid foci were tracked with MicroTracker (17), and mean squared displacement plots were created using MatLab scripts.

AlfA was purified for TIRF assays, light scattering, pelleting, and negative-stain electron microscopy as described (12). AlfB was expressed with a tobacco etch virus-cleavable 6His fusion and purified by affinity. Full materials and methods (26–30) are provided in the *SI Appendix*.

ACKNOWLEDGMENTS. We thank A. Derman and J. Pogliano (University of California, San Diego) for strains, plasmids, instruction on microbiological technique, and many invaluable conversations. We also thank K. C. Huang (Stanford University), A. Gopinathan (University of California, Merced), and E. C. Garner (Harvard University) for helpful discussions. This work was funded by National Institutes of Health Grants R01GM095263 and R01GM079556 (to R.D.M.) and by National Science Foundation and Genentech Graduate Research Fellowships (to J.K.P.).

1. Jones LJ, Carballido-López R, Errington J (2001) Control of cell shape in bacteria: Helical, actin-like filaments in Bacillus subtilis. *Cell* 104(6):913–922.
2. Derman AI, et al. (2009) Phylogenetic analysis identifies many uncharacterized actin-like proteins (Alps) in bacteria: Regulated polymerization, dynamic instability and treadmilling in Alp7A. *Mol Microbiol* 73(4):534–552.
3. Garner EC, et al. (2011) Coupled, circumferential motions of the cell wall synthesis machinery and MreB filaments in B. subtilis. *Science* 333(6039):222–225.
4. Domínguez-Escobar J, et al. (2011) Processive movement of MreB-associated cell wall biosynthetic complexes in bacteria. *Science* 333(6039):225–228.
5. van Teeffelen S, et al. (2011) The bacterial actin MreB rotates, and rotation depends on cell-wall assembly. *Proc Natl Acad Sci USA* 108(38):15822–15827.
6. Komeili A, Li Z, Newman DK, Jensen GJ (2006) Magnetosomes are cell membrane invaginations organized by the actin-like protein MamK. *Science* 311(5758):242–245.
7. Ma X, Ehrhardt DW, Margolin W (1996) Colocalization of cell division proteins FtsZ and FtsA to cytoskeletal structures in living Escherichia coli cells by using green fluorescent protein. *Proc Natl Acad Sci USA* 93(23):12998–13003.
8. Møller-Jensen J, Jensen RB, Löwe J, Gerdes K (2002) Prokaryotic DNA segregation by an actin-like filament. *EMBO J* 21(12):3119–3127.
9. Garner EC, Campbell CS, Weibel DB, Mullins RD (2007) Reconstitution of DNA segregation driven by assembly of a prokaryotic actin homolog. *Science* 315(5816):1270–1274.
10. Gayathri P, et al. (2012) A bipolar spindle of antiparallel ParM filaments drives bacterial plasmid segregation. *Science* 338(6112):1334–1337.
11. Becker E, et al. (2006) DNA segregation by the bacterial actin AlfA during Bacillus subtilis growth and development. *EMBO J* 25(24):5919–5931.
12. Polka JK, Kollman JM, Agard DA, Mullins RD (2009) The structure and assembly dynamics of plasmid actin AlfA imply a novel mechanism of DNA segregation. *J Bacteriol* 191(20):6219–6230.
13. Popp D, et al. (2010) Polymeric structures and dynamic properties of the bacterial actin AlfA. *J Mol Biol* 397(4):1031–1041.
14. Fuesler JA, Li H-J (2012) Dynamic instability—A common denominator in prokaryotic and eukaryotic DNA segregation and cell division. *Cell Mol Biol Lett* 17(4):542–548.
15. Tanaka T, Ogura M (1998) A novel Bacillus natto plasmid pLS32 capable of replication in Bacillus subtilis. *FEBS Lett* 422(2):243–246.
16. Campbell CS, Mullins RD (2007) In vivo visualization of type II plasmid segregation: bacterial actin filaments pushing plasmids. *J Cell Biol* 179(5):1059–1066.
17. Jaqaman K, et al. (2008) Robust single-particle tracking in live-cell time-lapse sequences. *Nat Methods* 5(8):695–702.
18. Weber SC, Spakowitz AJ, Theriot JA (2010) Bacterial chromosomal loci move subdiffusively through a viscoelastic cytoplasm. *Phys Rev Lett* 104(23):238102.
19. Tanaka T (2010) Functional analysis of the stability determinant AlfB of pBET131, a miniplasmid derivative of bacillus subtilis (natto) plasmid pLS32. *J Bacteriol* 192(5): 1221–1230.
20. Flyvbjerg H, Jobs E, Leibler S (1996) Kinetics of self-assembling microtubules: An "inverse problem" in biochemistry. *Proc Natl Acad Sci USA* 93(12):5975–5979.
21. Theriot JA (2013) Why are bacteria different from eukaryotes? *BMC Biol* 11:119–135.
22. Rivera CR, Kollman JM, Polka JK, Agard DA, Mullins RD (2011) Architecture and assembly of a divergent member of the ParM family of bacterial actin-like proteins. *J Biol Chem* 286(16):14282–14290.
23. Fisher AJ, Rosenstiel TN, Shirk MC, Fall R (2001) Nonradioactive assay for cellular dimethylallyl diphosphate. *Anal Biochem* 292(2):272–279.
24. McCabe BC, Gollnick P (2004) Cellular levels of trp RNA-binding attenuation protein in Bacillus subtilis. *J Bacteriol* 186(15):5157–5159.
25. Edelstein A, Amodaj N, Hoover K, Vale R, Stuurman N (2001) *Current Protocols in Molecular Biology* (John Wiley & Sons, New York).
26. van den Ent F, Löwe J (2006) RF cloning: A restriction-free method for inserting target genes into plasmids. *J Biochem Biophys Methods* 67(1):67–74.
27. Stuurman N, Edelstein AD, Amodaj N, Hoover KH, Vale RD (2010) Computer control of microscopes using μManager. *Curr Protoc Mol Biol* 92(Suppl):14.20.2–14.20.17.
28. Rygus T, Scheler A, Allmansberger R, Hillen W (1991) Molecular cloning, structure, promoters and regulatory elements for transcription of the Bacillus megaterium encoded regulon for xylose utilization. *Arch Microbiol* 155(6):535–542.
29. Vagner V, Dervyn E, Ehrlich SD (1998) A vector for systematic gene inactivation in Bacillus subtilis. *Microbiology* 144(Pt 11):3097–3104.
30. Ingerman E, Hsiao JY, Mullins RD (2013) Arp2/3 complex ATP hydrolysis promotes lamellipodial actin network disassembly but is dispensable for assembly. *J Cell Biol* 200(5):619–633.

SUPPLEMENTARY MATERIALS

Materials and Methods

Figures S1-S7

Tables S1-S7

Movies S1-S5

Materials and Methods

Plasmid and strain construction. The basis of many plasmids in this study was a fragment (Table S2) from pWH1520 containing an *E. coli* origin and ampicillin resistance gene, as well as a *B. subtilis* tetracycline resistance gene. This fragment was amplified by PCR using oligos JP0001 and JP0003 (Table S1), then digested with BamHI, and ligated together. To make pJKP01 (Table S2), *repN*, the origin of replication from pLS32 was amplified from pBET131 (11) with oligos JP0036 and JP0037 (Table S1) and cloned into the modified pWH1520 backbone with NsiI. To make pJKP02 and all other *lacO* array containing plasmids, as a final cloning step, the smaller BamHI fragment from pRL153 (2) was ligated into the BamHI site of pJKP01. To make pJKP03, the *alf* operon was amplified from pBET131 (11) with JP0043 and JP0044 and cloned into pJKP01 with restricition-free cloning (24). To make pJKP04, GFP from pMUTIN (27) was first amplified with JP0048 and JP0049 and cloned into a native BseRI site downstream of AlfA in pJKP03. Next, the AlfA-GFP region on this intermediate plasmid was amplified with JP0052 and JP0053, with KpnI and XmaI sites on these oligos permitting ligation to a PCR product containing essentially all of pJKP03, with KpnI and XmaI sites added with JP0050 and JP0051 downstream of the native *alf* operon. Thus, the product, pJKP04, has a second copy of AlfA which is a C-terminal GFP fusion downstream of the AlfC, but upstream of native transcriptional terminators. To make strains PY79 lacI-GFP and PY79 lacI-mCherry (Table S3), the relevant fluorescent proteins were amplified from pMUTIN (27) and pEImCherry with JP0082 and JP0083, and JP0086 and JP0087, respectively. These fragments were cloned into the SpeI and EagI sites of pEB387. This plasmid was then transformed using standard procedures to integrate into the AmyE locus of PY79 (Bacillus Genetic Stock Center).

To make pJKP104, for recombinant expression of AlfB, oligos JP0152 and JP0153 were used to amplify the coding sequence of an *E. coli*-optimized AlfB gene (Mr. Gene). The insert was then digested with PciI and XhoI for cloning into a pETM-11 vector (EMBL), generating a TEV-cleavable 6H tag on the N-terminus.

To make bundling-deficient mutants of AlfA in *Bacillus* and *E. coli* constructs (for protein purification), site-directed mutagenesis was employed, using primers JP0142-JP0145, JP0158-JP0163, and JP0201-JP0202 as described in Table S1.

Plasmid stability assay. Cells were grown to exponential phase (A600 of approximately 0.2-0.4) in LB in the presence of relevant antibiotics (10µg/ml tetracycline). Cells were harvested and resuspended in LB without antibitiotics, and 100µl of a $1:10^4$ dilution of cells was plated on LB plates, also free of antibiotic. Cultures were thus maintained in LB alone for 12-30 generations at 25, 30, or 37° by making 1:60 back-dilutions when A600 reached 0.2-0.4. At the end of the experiment, cells were plated on LB plates as

described above, and the actual number of generations passed calculated from final OD and total dilution factor over the course of the experiment. The following day, colonies were picked through the center of the colony to LB + 10µg/ml tetracycline plates. The fraction of resistant colonies before (r_0) and after (r_{final}) growth in LB was related to the number of generations (g) that had surpassed by an exponential decay function to obtain the loss rate (L).

$$r_{final} = r_0 \, e^{-(1-L)\,g}$$

Live cell imaging and tracking. *Bacillus subtilis* cells were grown in CH media to an A600 of roughly 0.2, then spun down and spotted to 1% agarose in CH polymerized into a cut pad in concavity slide (2). Images were acquired in oblique TIRF on a Nikon TE 2000 inverted microscope controlled with MicroManager (23) as described (12). Plasmid foci were tracked with MicroTracker (16) and mean squared displacement plots were created using MatLab scripts.

Images were bleach-corrected using an ImageJ macro (J. Reitdorf, EMBL).

Calculation of cellular concentration of AlfA and AlfB. Using estimates of 5e+8 cells/OD1 (21), our cultures at A600 of 0.5 contained 2.5e+8 cells/ml. Loading 10ul of this gives, assuming a cytoplasmic volume of 1e-14 liters per cell (25) 2.5e-8 liters of cytosol per well.

(5e+8 cells/OD1*ml) *0.01 ml * OD0.5 * 1e-14 L/cell = 2.5e-8 L cytosol per well.

1e-5 L (10µl) of purified standards were loaded, or 4e+2-fold in excess of the volume of cells. Given that the AlfA band is roughy equivalent to 50nM of this protein, the cellular concentration of protein must be approximately 50nm * 4e+2 or 20µM. The concentration of AlfB is based off the intensity of the AlfA band.

AlfA and AlfB protein purification. AlfA was purified as previous described (12). A codon-optimized AlfB was subcloned into a pETM11 plasmid so as to produce a C-terminal TEV-cleavable 6His tag as described above. After expression in C43 cells grown in TPM at 22 for 18 hours, cells were harvested, resuspending in lysis buffer (600mM KCl, 25mM Sodium phosphate pH 7.5, 1mM $MgCl_2$, 0.5mM βME, 10mM imidazole) and lysed with an Emulsiflex. After a high-speed clearing spin, the supernatant was passed through a 5ml Ni-NTA chelating column (Qiagen) continuously for 90 minutes at 4° C. The resin was then washed with 10 volumes of wash buffer (600mM KCl, 25mM Sodium phosphate pH 7.5, 1mM $MgCl_2$, 0.5mM βME, 100mM imidazole), and eluted with a 0-100% gradient of elution buffer (600mM KCl, 25mM Sodium phosphate pH 7.5, 1mM $MgCl_2$, 0.5mM βME, 250mM imidazole) on an AKTA Purifier (GE). The peak fractions were pooled and dialyzed back into lysis buffer. TEV protease was added overnight at a 1:100 molar ratio to the AlfB, and this digest passed for 90 minutes over the chelating column with the peristaltic pump to remove TEV and the 6His tag. The flowthrough was gel filtered on a 300ml S200 column, and stored at -80° C in lysis buffer + 20% glycerol.

Generation of *parN* reagents. Short, unlabeled constructs (1x-6x and "scramble") in Table S6 were ordered as reverse-complementing oligo pairs and annealed by stoichiometric mixing, heating to 95 degrees, and cooling by 10 degree increments over the course of 30 minutes. *parC* and labeled *parN* were generated by PCR, using biotin or Cy3 labeled primers as required. To make multivalent particles for TIRF, magnetic beads (Bangs labs) were labeled with biotin- and Cy3- labeled *parN* as described (9).

These beads were sedimented and the supernatant collected, with absorbance at the Cy3 peak used to determine DNA concentration.

Light scattering. Proteins were mixed using a SFA-20 stopped flow device in a K2 ISS fluorimeter as described (12), except for the experiments described in Figure S5, which were performed by manual mixing in a Varian Cary Eclipse fluorescence spectrophotometer.

Negative stain EM. Negative staining was carried out as described (12).

TIRF microscopy. APTES and PEG-NHS functionalized coverslips were produced as described (12), with the counter glass passivated with DEDC silane as described (9). Approximately 20 seconds after adding ATP to a reaction on a passivated slide, a functionalized coverslip was dropped on top and immediately sealed with VALAP (molten mixture of Vaseline, lanolin, and paraffin at 1:1:1 mass ratio). Samples were then imaged on a Nikon Eclipse TE2000-E inverted microscope, illuminated by a 100-MW 542 solid-state laser and a 40-mW 488/514 argon ion laser in TIRF. Images were captured on an Andor iXon EM CDD.

Images were background subtracted with a rolling ball radius of 30 pixels in ImageJ. For supplemental movies, images were scaled 2x with bilinear interpolation.

Table S1. Oligos used in this study.

Name	Purpose	Template	Sequence
JP0001	Making mini pWH1520 with BamHI site	pWH1520	aaaa ggatcc ATGGAACGGGTTGGCATGG
JP0003	Making mini pWH1520 with BamHI site	pWH1520	aaaa ggatcc TATTGTTGTATAAGTGATGAAATACTGAATTTAA
JP0036	Adding OriN with NsiI site (making pJKP01)	pBET131	TTGA ATGCAT cagaagaatatgtagaag
JP0037	Adding OriN with NsiI site (making pJKP01)	pBET131	TTGA ATGCAT agcttcctcctaaaatc
JP0043	Adding alf operon (restriction-free cloning) (making pJKP03)	pBET131	tgctcgccgaggcggcataaatcg ggatcc GAATTTAGGTAAAAATTTAAT
JP0044	Adding alf operon (restriction-free cloning) (making pJKP03)	pBET131	actagtactaataaaattaatcat AGAAAAAATATTTTTTCTGTT
JP0048	Adding GFP downstream of AlfA with native BseRI site	pMUTIN	TAAT GAGGAGATGTTTGCGTTA GCTAGCAAAGGAGAAGAACTT

JP0049	Adding GFP downstream of AlfA with native BseRI site	pMUTIN	ACTCACtactggTaCTCCTCTCATTTGTAGAGC TCATCCATGCC
JP0050	Adding second copy of AlfA downstream of *alf* operon (with XmaI and KpnI sites)	pJKP03	atta CCCGGG agacagccaaaaggctgtctt
JP0051	Adding second copy of AlfA downstream of *alf* operon (with XmaI and KpnI sites)	pJKP03	attgGGTACCttattcttcgttcctaattat
JP0052	Adding second copy of AlfA downstream of *alf* operon (with XmaI and KpnI sites)	AlfA-GFP from JP0048, JP0049	caat GGTACC gagttccaactaaagaaaact
JP0053	Adding second copy of AlfA downstream of *alf* operon (with XmaI and KpnI sites)	AlfA-GFP from JP0048, JP0049	taatCCCGGGaataaagacagccttttggct
JP0082	Replacing CFP in pEB387 with GFP	pMUTIN	tt ACTAGT AAAGGAGAAGAACTTTTC
JP0083	Replacing CFP in pEB387 with GFP	pMUTIN	cata CGGCCG TTTGTAGAGCTCATCCAT
JP0086	Replacing CFP in pEB387 with mCherry	pEImCherry	tt ACTAGT aagggcgaggaggataacatg
JP0087	Replacing CFP in pEB387 with mCherry	pEImCherry	cata CGGCCG cttgtacagctcgtccatgcc
JP0142	Site directed mutagenesis of AlfA KK101AA	pJKP100	CCATTTTCAAAGAAACCGGCGCAGCGGAG TTCAACCTGATTCTG
JP0143	Site directed mutagenesis of AlfA KK101AA	pJKP100	CAGAATCAGGTTGAACTCCGCTGCGCCGGT TTCTTTGAAAATGG
JP0144	Site directed mutagenesis of AlfA KK21AA	pJKP100	GAAGTACGCATATAAGGACGCCGCGCAGA TCAAGGTTGGTAGC
JP0145	Site directed mutagenesis of AlfA KK21AA	pJKP100	GCTACCAACCTTGATCTGCGCGGCGTCCTT ATATGCGTACTTC
JP0152	Met-Ser (to make PciI site) for cloning AlfB into pETM11 (6His TEV)	Codon optimized AlfB	TTCC ACATGT cc CGTGAAGACAACTTTATGTACCAG

JP0153	XhoI for cloning AlfB into pETM11 (6His TEV)	Codon optimized AlfB	GGAACTCGAGTCATCACAGGAAACCACCAGAATCGTC
JP0158	Site directed mutagenesis of AlfA KK21DD	pJKP100	CTACGAAGTACGCATATAAGGACGATGATCAGATCAAGGTTGGTAGCTTCCC
JP0159	Site directed mutagenesis of AlfA KK21DD	pJKP100	GGGAAGCTACCAACCTTGATCTGATCATCGTCCTTATATGCGTACTTCGTAG
JP0160	Site directed mutagenesis of AlfA KK101DD	pJKP100	CACCATTTTCAAAGAAACCGGCGACGACGAGTTCAACCTGATTCTGACC
JP0161	Site directed mutagenesis of AlfA KK101DD	pJKP100	GGTCAGAATCAGGTTGAACTCGTCGTCGCCGGTTTCTTTGAAAATGGTG
JP0162	Site directed mutagenesis of AlfA KK21DD (making pJKP08)	pJKP03	GTACGAAGTACGCTTATAAGGACGACGACCAAATTAAGGTCGGCAGTTTCC
JP0163	Site directed mutagenesis of AlfA KK21DD (making pJKP08)	pJKP03	GGAAACTGCCGACCTTAATTTGGTCGTCGTCCTTATAAGCGTACTTCGTAC
JP0201	Site directed mutagenesis of AlfA KK101DD (making pJKP08)	pJKP03	GAGACTGGAgAcgAcGAATTTAACttaattctaacttgcccatatgaaagtatgg
JP0202	Site directed mutagenesis of AlfA KK101DD (making pJKP08)	pJKP03	GTTAAATTCgTcgTcTCCAGTCTCtttaaagattgtatagagagcatatactaatcgaatttgacct

Table S2. Plasmids used in this study.

Name	**Description**	**Backbone/source**	**Purpose**
pJKP01	Mini pWH1520 derivative	pWH1520	Control plasmid for plasmid maintenance assay
pJKP02	pJKP01 + lacO	pJKP01	Control plasmid for visualization of plasmids
pJKP03	pJKP01 + *alf*	Mini	Plasmid maintenance assay
pJKP04	pJKP03 + alfA-GFP	Mini + alf	Visualization of filaments with second copy of AlfA fused to GFP

pJKP06	pJKP04 lacO	Mini + alf + GFP	Visualization of plasmid and filaments with second copy of AlfA fused to GFP
pJKP08	pJKP03 (KK21DD, KK101DD)	Mini + alf	Effect of bundling on partioning
pJKP10	pJKP03+lacO	Mini + alf	Visualization of plasmids
pJKP50	P_{xylA} lacI-GFP	pEB387	Making chromosomal integrations of lacI
pJKP51	P_{xylA} lacI-mCherry	pEB387	Making chromosomal integrations of lacI
pJKP100	Codon-optimized AlfA	pET20b	Expression and purification of AlfA (12)
pJKP101	As above with GSKCK appended to C terminus	pET20b	Expression and purification of AlfA for maleimide labeling (12)
pJKP102	As pJKP100 with KK21AA and KK101AA	pET20b	Expression and purification of non-bundling AlfA
pJKP103	As pJKP100 with KK21DD and KK101DD	pET20b	Expression and purification of non-bundling AlfA
pJKP104	6H-TEV-AlfB	pETM11	Expression and purification of AlfB
pNCH106	pNCH106 AlfA-GFP	(11)	Visualization of AlfA filament dynamics
pRL153	lacO array	(2)	Cloning the lacO array
pEB387	P_{xylA} lacI	(2)	*AmyE* integration vector
pWH1520	Shuttle vector	(26)	Basis of pJKP01
pMUTIN-GFP	Systematic gene inactivation in *B. subtilis*	(27)	Amplification of GFP
pEImCherry	N/A	(28)	Amplification of mCherry
pBET131	7kb *alf* operon	(11)	Amplification of the *alf* operon and *oriN* origin of replication region

Table S3. Strains used in this study.

Name	Genotype	Purpose
PY79	Prototroph, 168 lineage	Plasmid maintenance assay
PY79 mCherry-lacI	PY79 *amyE::(P_{xyl}mCherry-lacI)*	Visualization of filaments and plasmids
PY79 GFP-lacI	PY79 *amyE::(P_{xyl}mGFP-lacI)*	Visualization of plasmids only

Figure S1: Diagram of the *alf* operon

parN is a DNA region comprised of 3 tandem repeats of an 8bp AT-rich sequence. It surrounds the promoter of the operon, and binding of AlfB to *parN* suppresses transcription of the operon (18). Downstream of AlfB is a third open reading frame of unknown function.

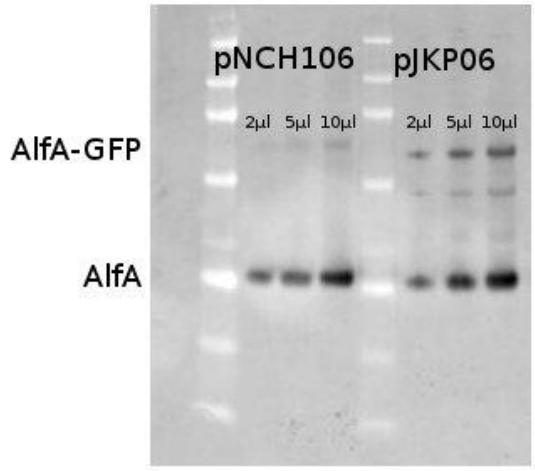

Figure S2: Quantification of AlfA to AlfA-GFP ratio in pJKP04 and pNCH106 (in PY79)

Antisera against purified recombinant AlfA and AlfB were raised in New Zealand White Rabbits (Pacific Immunology). Extracts of Bacillus subtilis PY79 cells containing pJKP06 or pNCH106 grown to OD600 of approximately 0.5 were freeze-thawed and bath sonicated for 10 minutes in the presence of 1mM EDTA and 1mM DTT. After boiling and centrifugation in the presence of sample buffer, 2, 5, and 10µl of sample, respectively, were loaded to a gel. These blots with incubated with antisera at 1:10 and Alexa 488

anti-rabbit goat IgG secondary at 1:4000 (Invitrogen) before imaging on a Typhoon Imager (GE). In pNCH106, AlfA-GFP is present at 7% (+/- 2%) of the endogenous AlfA, while in pJKP06, AlfA-GFP is present at 25% (+/- 2%) of endogenous AlfA.

Table S4. Rates of plasmids loss

Miniplasmid	**Loss rate/generation**	**N**
pJKP01 (Origin only)	6.06%	2
pJKP03 (+alf)	0.59%	5
pJKP04 (+alf w/2nd AlfA-GFP)	1.35%	2
pJKP08 (KK21DD, KK101DD alf)	1.47%	1

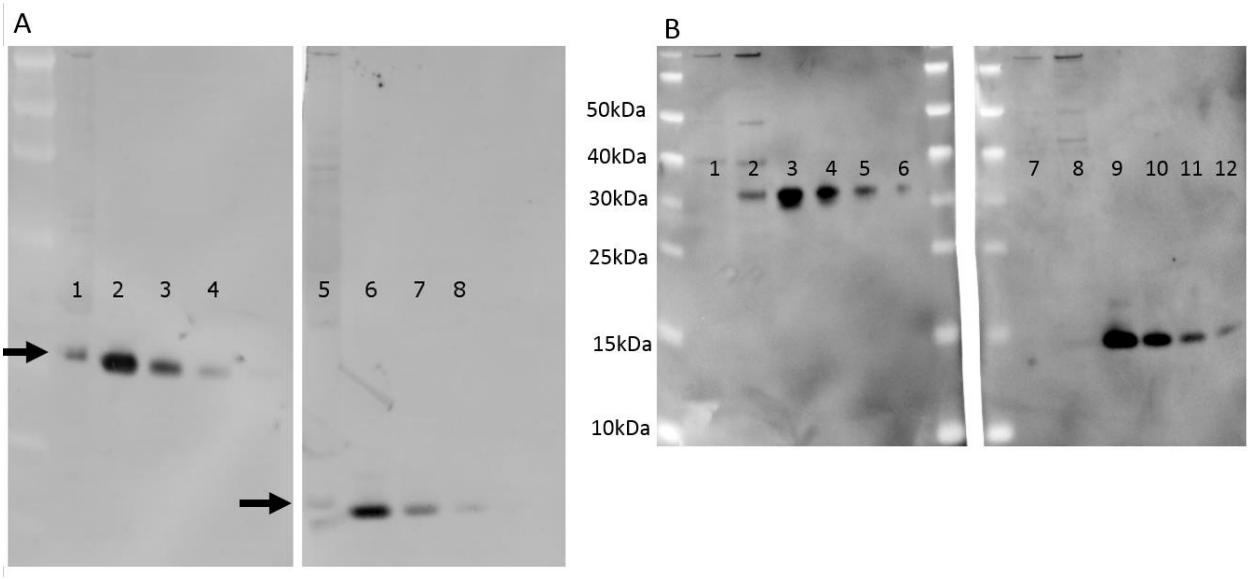

Figure S3: Quantification of cellular ratio of AlfA:AlfB.

Antisera against purified recombinant AlfA and AlfB were raised in New Zealand White Rabbits (Pacific Immunology). (A) An extract of Bacillus subtilis PY79 cells containing pJKP03 grown to OD600 of 0.523 was freeze-thawed and bath sonicated for 10 minutes in the presence of 1mM EDTA and 1mM DTT. After boiling and centrifugation in the presence of sample buffer, an equal volume of this extract (lanes 1 and 5) was loaded next to defined concentrations of purified protein (300nM, 100nM, 30nM AlfA in lanes 2-4, and equivalent concentrations of AlfB in lanes 6-8). These blots with incubated with antisera at 1:10 and Alexa 488 anti-rabbit goat IgG secondary at 1:4000 (Invitrogen) before imaging on a Typhoon Imager (GE). (B) Western blot performed with chemiluminescence. Lanes 1-6 were blotted with Anti-AlfA serum, and lanes 7-12 with anti-AlfB. Lanes 1 and 7 contain pJKP01 (miniplasmid with no *alf* operon), lanes 2 and 8 pJKP03 (miniplasmid with *alf* operon), lanes 3-6 purified AlfA standards, and lanes 8-12 purified AlfB standards.

Table S5. Steady state monomer concentrations as measured by right angle light scattering

Conditions	Concentration (standard deviation)	N
AlfA	2.24µM (+/- 0.0455)	4
AlfA + 1.3µM AlfB	2.97µM (+/- 0.266)	3
AlfA + 6.5µM AlfB	3.36µM	1
AlfA + 1.3 µM AlfB + 50nM parN	1.59µM (+/- 0.326)	2

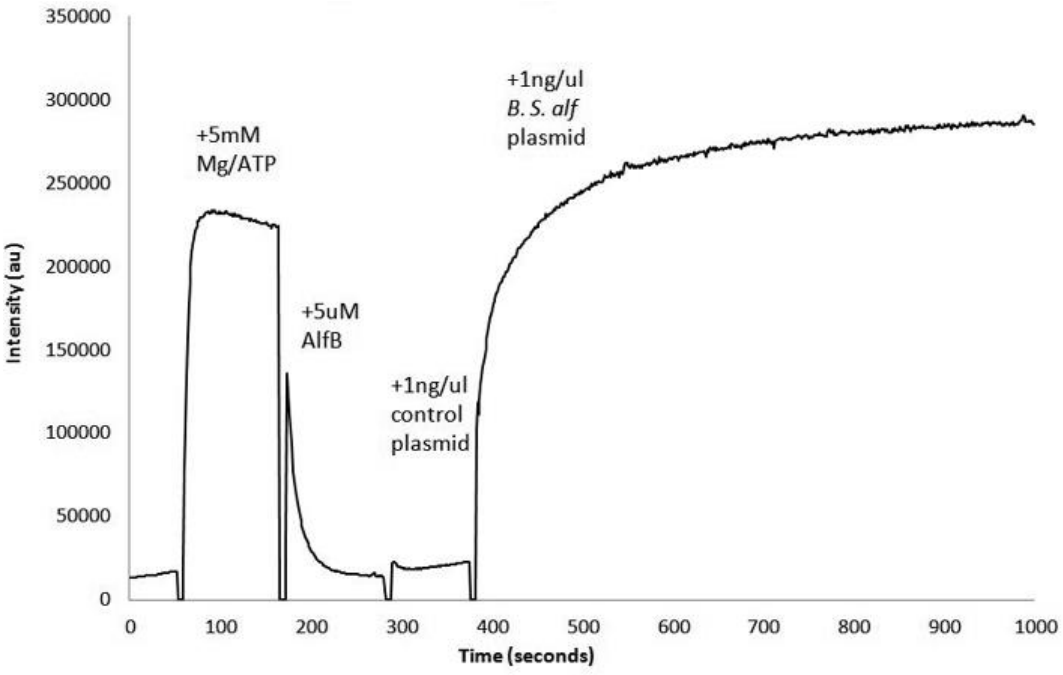

Figure S4: Effect of non-specific DNA on AlfA light scattering in the presence of AlfB. At time zero, the cuvette contained 5µM AlfA. At 60 seconds 5mM Mg/ATP was added, inducing polymerization. At approximately 180 seconds, 5µM AlfB was added, and the light scattering signal diminishes. At 300 seconds, addition of 1ng/µl nonspecific plasmid DNA (pETM11) does not dramatically change light scattering intensity. At 390 seconds, addition of the same concentration of *alf* plasmid (pJKP03) (containing *parN*) restores light scattering to levels higher than after initial addition of nucleotide. Conditions, 100mM KCl, 25mM Tris HCl pH 7.5, 1mM DTT, 1mM MgCl2. Temperature, 25˚ C.

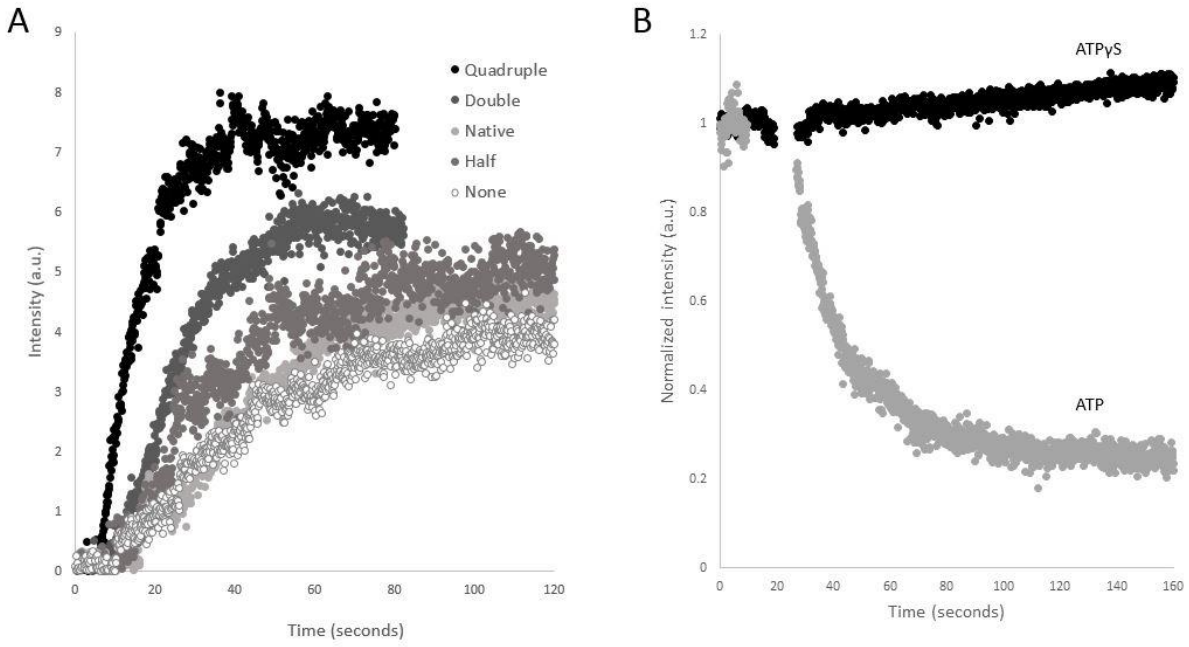

Figure S5: Effect of different *parN* repeat spacing on AlfA stabilization and interaction of AlfB with AlfA polymerized ATP and non-hydrolysable analogue (ATPγS). (A) 25nM of modified *parN* sequences ("short" sequences in Table S6) were added by manual mixing to a solution containing 2.1µM AlfA, 1.3µM AlfB, 5mM ATP. Background intensity (approximately 12 a.u. in each case) was subtracted. Buffer: 100mM KCl, 25mM Tris pH 7.5, 1mM $MgCl_2$, 1mM DTT. (B) 3µM of AlfA polymer was formed with 5mM ATP and 300µM ATP ATPγS using the ATP and AMPPNP critical concentrations previously reported (12). 1.3µM AlfB was added at time ~30 seconds. Traces were normalized to maximum intensities after background subtraction (Intensity values of unpolymerized AlfA, 3µM of AlfA polymer made with ATP, and 3µM of AlfA made with ATPγS were approximately 52, 82, and 300 a.u., respectively).

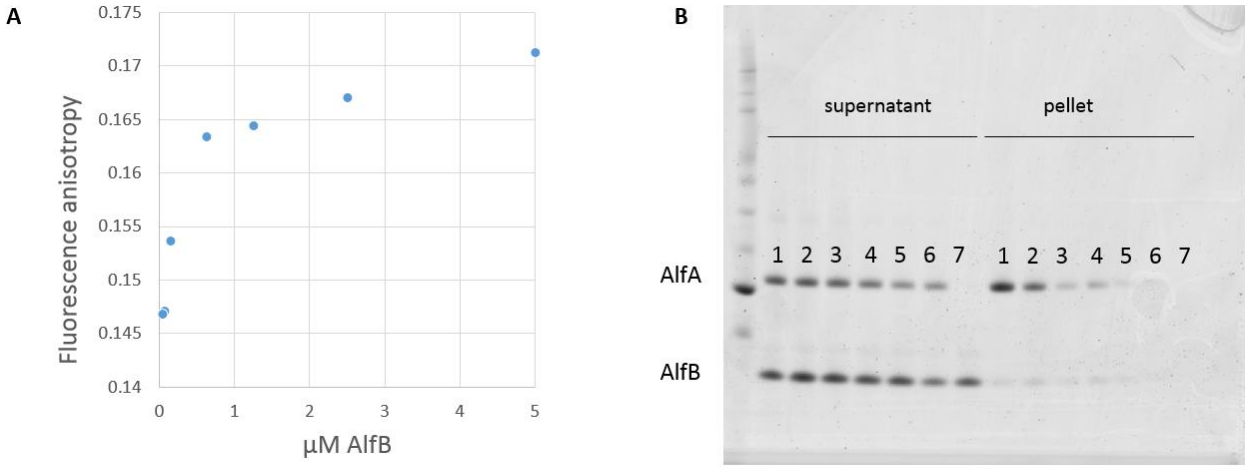

Figure S6. Interaction of AlfB with monomeric and polymeric AlfA.

(A) Fluorescence anisotropy created by AlfB binding to monomeric AlfA. 1µM Alexa-488 labeled AlfA well below its critical concentration in the presence of 2mM ATP was mixed with varying concentrations of AlfB, and the fluorescence anisotropy measured. Conditions, 100mM KCl, 25mM Tris HCl pH 7.5, 1mM DTT, 1mM MgCl2. Temperature, 25˚ C. (B) AlfB cosediments with AlfA polymers. Reactions 1-7 contain 10µM AlfB and 5mM ATP in the presence of 10µM, 6.4µM, 5.1µM, 4.1µM, 3.2µM, 2.6µM, and 0µM AlfA, respectively. After incubating the reactions at room temperature for 10 minutes, they were centrifugation at 80,000rpm (278,000 rcf) for 20 minutes at room temperature in a TLA 100 rotor. AlfB appears in pellet fractions only in the presence of AlfA. Conditions, as above.

Table S6. *parN* truncations, extensions, and spacing modifications. AlfB binding sites (18) are highlighted in bold.

Construct	**Sequence**
3x (native *parN*)	gcgattagataataa**tttatttaa**gag**tttatttaa**aaaa**attatttaa**cgtatgaataacttt
6x	gcg**tttatttaaa**gag**tttatttaa**cccc**attatttaa**cgttaa**tttatttaa**ctcc**tttatttaa**ggag**attatttaa**ggc
2x	gattagataataa**tttatttaa**gag**tttatttaa**cgtatgaataacttt
1x	gattagataataa**tttatttaa**cgtatgaataacttt
Scramble	ataagtatatttcttattatgaaaagttgagtaatcaaatcagattatattaaatattgttt
(Cy3-) parN-biotin	cattttttcattttgcgattagataataatttatttaagagtttatttaaaaaattatttacgtatgaataactttccattataattga aatgagttccaactaaagaaaactaaggag
parC	Cggataacaattcccctctagaaataattttgtttaactttaagaaggagatata**catatg**cactttgttacccgcc**aaaac aaaacccaaaaacaacccatacccaacccaataaaacaccaaaacaagaca**aataatcattgattgatggttga aatggggtaaacttga**caaacaaacccacttaaaacccaaaacatacccaaacacacaccaaaaaaacacc**at aaggagttttataaatgttg**ggatcc**ggctgctaacaaagcccgaaagga
Short (native)	taataa**tttatttaa**gag**tttatttaa**aaaa**attatttaa**cgtatg
Short, no spaces	taataa**tttatttatttatttaattatttaa**cgtatg
Short, half spaces	taataa**tttatttaa**g**tttatttaa**aa**attatttaa**cgtatg
Short, double spaces	taataa**tttatttaa**cgagagg**tttatttaa**ggaaaacc**attatttaa**cgtatg

Short, quadruple spaces	taataa**tttatttta**aaaacgagag**gaagaa****tttattta**aaaaggaaaacaacaa**attatttta**cgtatg

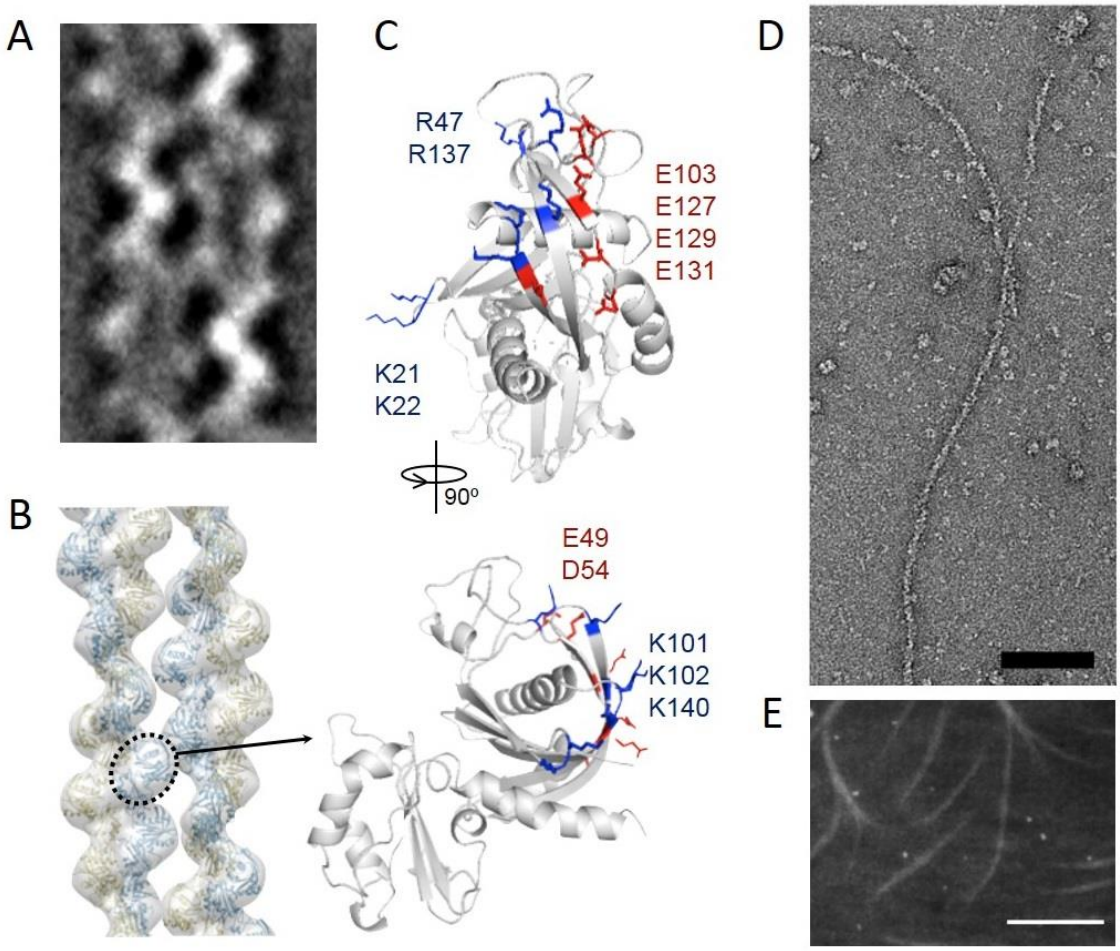

Figure S7. Design and validation of the bundling-deficient K21,K22,K101,K102 mutants

A helical reconstruction of AlfA filaments as described in (12) was fit to reference free-averages of two-filament bundles (A). A homology model of AlfA based on the ParM crystal structure was fit into this (B) and charged residues likely to be involved in bundling were identified, shown highlighted in red and blue (C). Mutation of two pairs of lysine residues (K21, K22, K101, K102) to alanine produced filaments which do not bundle under non-crowded conditions (D, scale bar 50nm). However, in crowded conditions (1mg/ml BSA, 0.4% methylcellulose) this mutant (10% KK21AA,KK101AA-KCK-biotin, 10% KK21AA,KK101AA-KCK-Alexa-488) forms bundles (E, scale bar 10µm).

Table S7. Manually scored behaviors of neighboring DNA particles on same AlfA structure in first frames of TIRF assay.

Behavior	**Pairs (n = 231)**
Filament severs or DNA disappears	10%
Maintain distance	13%
Pushed together	17%
Pushed apart	60%

Supporting Information

Polka et al. 10.1073/pnas.1304127111

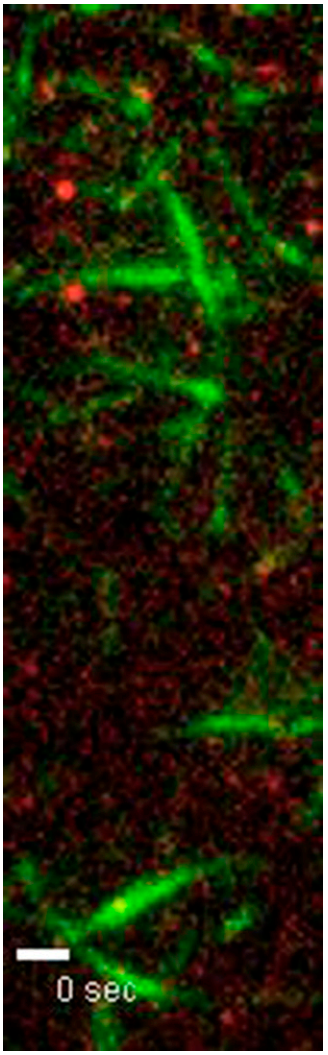

Movie S1. DNA-bound AlfA filaments are more dynamic than unbound filaments: 6 nM *parN*, 3 μM AlfA, 1.5 μM AlfB. (Scale bar, 1 μm.) Acquisition interval, 5 s.

Movie S1

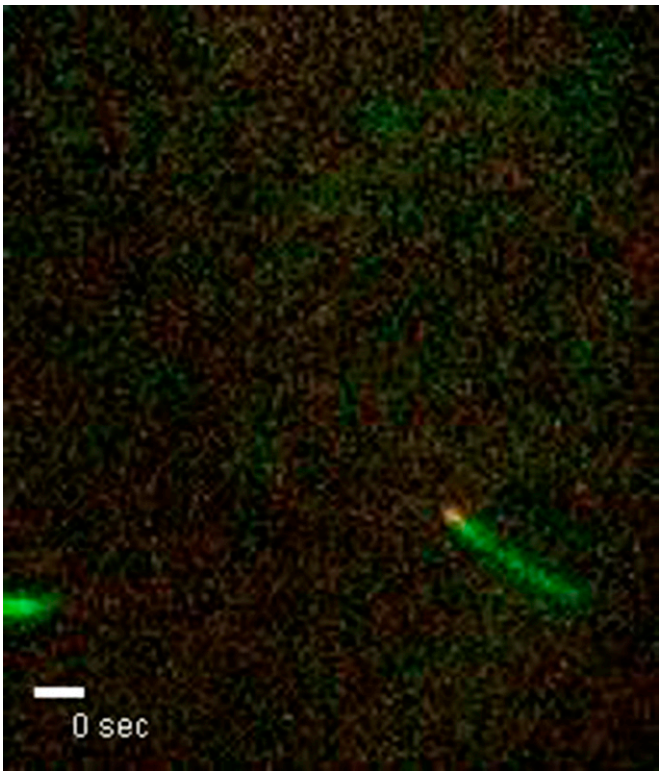

Movie S2. Multivalent *parN* particles can be propelled processively. Source for Fig. 4*C*: 20 nM *parN*, 3 μM AlfA, 1.5 μM AlfB. (Scale bar, 1 μm.) Acquisition interval, 5 s.

Movie S2

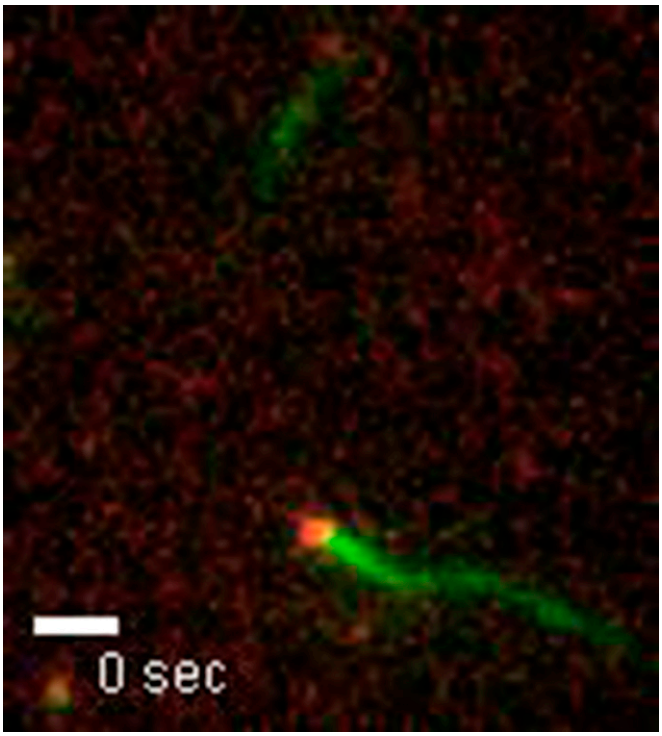

Movie S3. A *parN* particle breaks apart, with the daughters pushed in opposite directions. Source for Fig. 4*D*: 60 nM *parN*, 3.2 μM AlfA, 1.6 μM AlfB. (Scale bar, 1 μm.) Acquisition interval, 3 s.

Movie S3

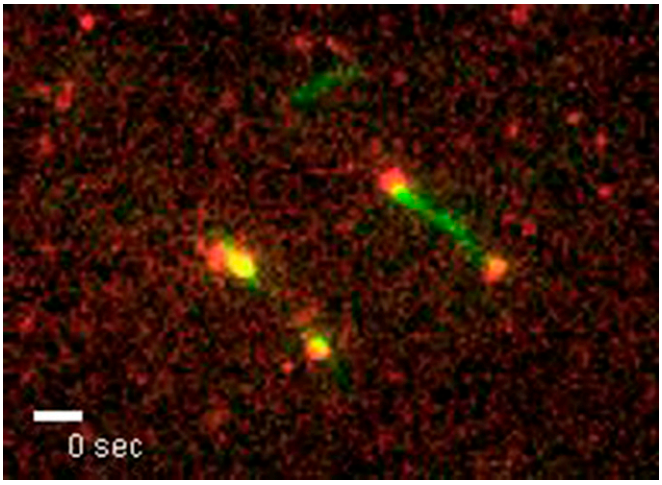

Movie S4. Multiple successive filament/DNA rearrangements and segregation events. Source for Fig. 4*E*: 60 nM *parN*, 3.2 μM AlfA, 1.6 μM AlfB. (Scale bar, 1 μm.) Acquisition interval, 3 s.

Movie S4

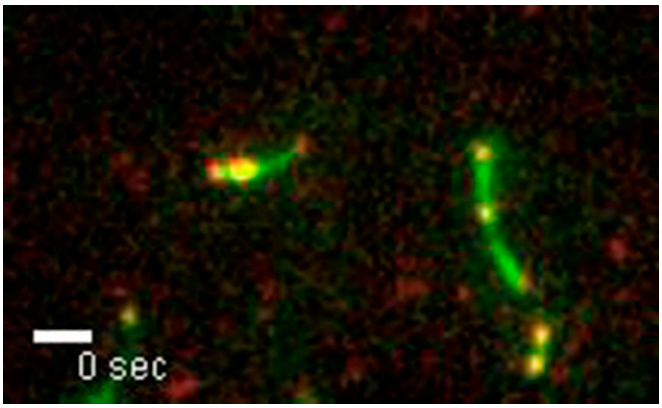

Movie S5. Multiple successive filament/DNA rearrangements and segregation events: 60 nM *parN*, 3.2 μM AlfA, 1.6 μM AlfB. (Scale bar, 1 μm.) Acquisition interval, 3 s.

Movie S5

Other Supporting Information Files

SI Appendix (PDF)